International Journal of the Korean Society of Precision Engineering, Vol. 3, No 4, October 2002.

Robust Controller Design for a Stabilized Head Mirror

Joong-Eup Keh[1] and Man-Hyung Lee[2]

[1] Defense Quality Assurance Agency (DQAA), South Korea
[2] School of Mechanical Engineering, Pusan National University, Pusan, South Korea

ABSTRACT

In this paper, LMI (Linear Matrix Inequality) based on H_∞ controller for a line of sight (LOS) stabilization system. It shows that the proposed controller has more excellent stabilization performance than that of the conventional PI-Lead controller. An H_∞ control has been also applied to the system for reducing modeling errors and the settling time of the system. The LMI-based H_∞ controller design is more practical in view of reducing a run-time than Riccati-based H_∞ controller. This H_∞ controller is available not only to decrease the gain in PI-Lead control, but also to compensate the identifications for the various uncertain parameters. Therefore, this paper, shows that the proposed LMI - based H_∞ controller had good disturbance attenuation and reference input tracking performance compared with the control performance of the conventional controller under any real disturbances.

Keywords : Stabilization System, Line-of-Sight (LOS), Linear Matrix Inequality (LMI), Robust Control, Tracking, Disturbance, Gimbal System, H_∞ Controller, PI-Lead Controller

1. Introduction

Modern weapons system is precise sophisticated and automated as scientific techniques develop. A line of sight (hereafter we call it LOS) stabilization system mounted on ground vehicles is operated as both synthetic sensor package and mechanical stabilization system. Even though the vehicle is moving, its LOS stabilization system is used as a device which enables the operator to fire exactly for target recognition and detection. This LOS plays an important role in keeping recognition at the target and stably tracking the operator's handle command. The LOS stabilization system is thereby important in that it provides a stabilized LOS to operator and sends the target's position into fire control system [1]. In the guidance indication system, the LOS stabilization system enables the operator to control the gun and turret by tracking the target well [1-2]. These functions of the system is achieved to implement the angular velocity control this servo and stabilization function of system is loop by using gyro as an inertial sensor. Moreover, this servo and stabilization function of system is closely related with the magnitude of disturbance and the controller. The stabilization error of this system mounted on the ground vehicle lies in between 0.05mil and 0.25mil. There exist disturbances such as bearing friction, unbalance of mass, spring force by sensor and actuator and force occurred by the inertial moment and geometric relation. Among them, the friction is the main factor to decrease the tracking performance at low speed and the stabilization performance [3]. This LOS stabilization system plays an important role in increasing mark hitting rate by means of tracking the target well and stabilizing the LOS under the turret's and the vehicle's movement. Nowadays, this study on the given system has been continuously achieved in solving the overall disturbance problems plus the torque disturbance by the gun's elevation motion, improving the tracking performance and reducing the drift problem like a trouble shooting by the mirror's motion occurred in the errors of the velocity control system [1-6], and the references therein.

This paper is concerned with the design of an LMI -based H_∞ controller for the track vehicle. The control algorithm is also employed in view of dealing with the robustness against the factors such as nonlinear

characteristics, parametric change and modeling error.

This paper is organized into as follows. First, the descriptions on the structures of stabilized mirror and a LOS stabilization system, and the derivation of nonlinear equation of motion and mathematical modeling considered by dynamical characteristics.

Second, an LMI-based H^{∞} control theory is introduced and the many formulas are suggested to design the controller for the given system.

Finally, the formulation is performed to design the proper controller for this system and then the simulation is achieved for the performance in comparison with that of the conventional controller after the H^{∞} controller design for the specification

2. Characteristic and Structure of a LOS Stabilization System

2.1 Stabilization System

The gimbal is, as shown in Figure 2.1, composed of the gimbal housing, platform, stabilized mirror and inertial balancer and the object is observed through the stabilized mirror. Also, it uses the 2-axis driving mechanism. The gimbal system used in this study is a type of belt-driving, which has a simple mechanism and is able to employ the inertial balancer to improve the stabilization performance at elevation. The components is described as follows.

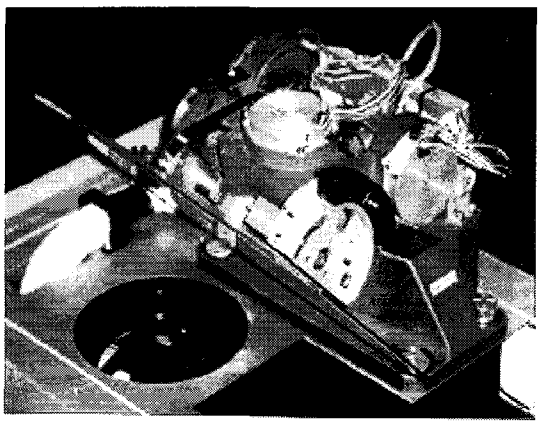

Fig. 2.1 A line of sight stabilization system

Electronic unit of stabilization system is activated by obtaining the voltages 24 V plus minus 6 V from the vehicle and is in charge of all works for stabilization. It basically judges the condition and the physical quantity obtained from the sensor and drives the motor by calculating the proper control quantity. As a result, the stabilized mirror is also controlled by the above sequence. Apart from the main servo components of system, the self-tests on the processors such as AD, DA converter and the initialization of system are also calculated. The overall network of system focused on a electronic device used for stabilization and servo control is shown in Figure 2.2.

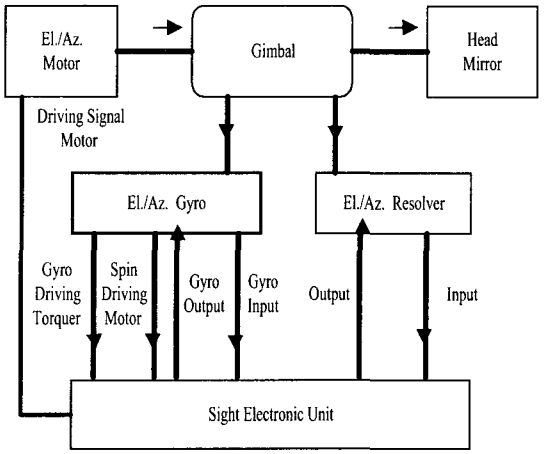

Fig. 2.2 Electronic network of stabilization system

2.2 Operation Modes of System

The driving program is performed from reset circuit's activation after the power is supplied to the system. Before the main program's execution, power-on self-test for the main assembly of stabilization system is performed and then the initialization works to execute the main program. The control of system starts after this initialization. If there are no faults in power-on self-test and system initialization, the main program can be executed. The operation mode is divided into three modes; stabilization, follow and aut o-drift compensating mode.

The stabilization mode is an angular velocity control loop driven by handle input command and the important operation mode mainly used in the vehicles motion. The specifications of design are shown in Table 2.1. The velocity control loop in a stabilization system can be shown as Figure 2.3.

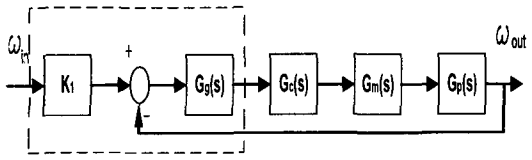

Fig. 2.3 Velocity control loop in a LOS stabilization system

Win/Wout : Input/Output of angular velocity,
Gg(s) : Gyro, **Gc(s)** : Controller,
Gm(s) : Motor, **Gp(s)** : System(Gimbal),
K1(s) : Precession Scale Factor(Gyro)

Table 2.1 Design performance of stabilization mode

Contents	Objectives
Bandwidth	Over 30Hz
Velocity of motion at elevation	Max. over 10°/sec Min. below 0.25mil/sec
Velocity of motion at azimuth	Max. over 40°/sec Min. below 0.25mil/sec
Stabilization accuracy	Below 0.1 mil RMS
Tracking accuracy	Below ±1.5% or ±0.3mil
Drift	Below 0.2 mil/sec
Acceleration capability	Over 3 rad/sec^2

The follow mode is operated on the time when the stabilization mode can't work normally or the initial adjustment of system is set up. Furthermore, this mode is an angle control loop which well tracks the command of ballistic trajectory calculator, sending the signal into the fire control system.

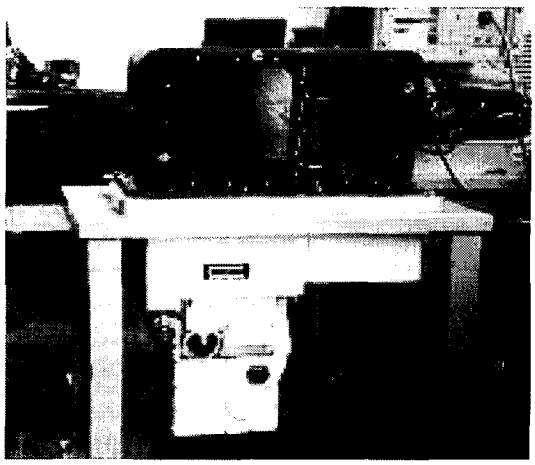

Fig. 2.4 Equipment setup for obtaining data

Figure 2.4 shows the experimental device setup for the comparison of step response between stabilization and follow mode and the data of experiments are shown by the oscilloscope and the plotter.

3. Mathematical Modeling

The gimbal is composed of the gimbal housing, platform, stabilized mirror and inertial balancer, where the gimbal housing mounted on the base structure moves at azimuth direction. The platform mounted on the gimbal housing rotates at elevation direction, which has the 2-axis gyro as the inertial sensor, and forms the angular velocity control loop stabilize the platform inertially. The stabilized mirror also mounted on the gimbal housing has the parallel rotation shaft with that of platform and moves at elevation direction. The stabilization at elevation is to keep the stabilized mirror into a half as much as this motion for the vehicle's azimuth motion and is achieved to control the platform by the gyro. Inertial balancer mounted on the gimbal housing moves at elevation. Its rotation shaft is equal to those of platform and stabilized mirror, and the platform is linked with the stabilized mirror by wire band. If there is no slip between inertial balancer and wire band, the inertial balancer stabilizes the platform inertially by the dynamic relations under no other forces. If considered with the kinetic energy of rigid bodies and the elastic energy of the wire band in order to derive the equation of motion, the following equation is obtained by using the Lagrange equation.

$$\frac{d}{dt}\left(\frac{\partial(T-V)}{\partial \dot{q}_i}\right)-\frac{\partial(T-V)}{\partial q_i}=Q_i. \qquad (3.1)$$

Before deriving the equation of motion, the following assumptions are made. First, there exists the center of weight of the gimbal housing, platform, stabilized mirror and inertial balancer on one plane. Second, the center of weight is in accordance with the center of rotation. Third, the velocity and the angular velocity can be measured.

3.1 Dynamic Equations

For convenience and derivation of equation, the rectangular coordinates attached to each rigid body are

used in this section. The kinetic energy of the overall gimbal system is represented as (3.2) by solving of the kinetic energy of each rigid body and using the existing kinematics and the angular velocity [3], and the references therein.

$$\begin{aligned} T &= T_G + T_P + T_M + T_B \\ &= \frac{1}{2} m_G \sum_{i=1}^{3} V_i^{G*} V_i^{G*} + \frac{1}{2} \sum_{i=1}^{3} G_i \omega_i^G \omega_i^G \\ &+ \frac{1}{2} m_p \sum_{i=1}^{3} V_i^{p*} V_i^{p*} + \frac{1}{2} \sum_{i=1}^{3} p_i \omega_i^p \omega_i^p \\ &+ \frac{1}{2} m_M \sum_{i=1}^{3} V_i^{M*} V_i^{M*} + \frac{1}{2} \sum_{i=1}^{3} M_i \omega_i^M \omega_i^M \\ &+ \frac{1}{2} m_B \sum_{i=1}^{3} V_i^{B*} V_i^{B*} + \frac{1}{2} \sum_{i=1}^{3} B_i \omega_i^B \omega_i^B \end{aligned} \tag{3.2}$$

T_G : Kinetic energy of the gimbal housing
T_p : Kinetic energy of the platform
T_M : Kinetic energy of the stabilized mirror
T_B : Kinetic energy of the inertia balancer

The potential energy of gimbal system is divided into two parts; one is an elastic energy V_k by wire band and the other is a potential energy V_g by gravity. Elastic energy by wire band and stiffness is represented as follows.

$$\begin{aligned} V_k = & \frac{1}{2} K_1 (r_p \theta_p - r_M \theta_M)^2 + \frac{1}{2} K_2 (r_B \theta_B - r_p \theta_p)^2 \\ & + \frac{1}{2} K_3 (r_M \theta_M - r_B \theta_B)^2 \end{aligned} \tag{3.3}$$

Also, the stiffness of wire band is given as

$$K_1 = \frac{EA}{L_1}, \quad K_2 = \frac{EA}{L_2}, \quad K_3 = \frac{EA}{L_3},$$

where E and A is the elasticity coefficient of wire band and area, and L_1, L_2 and L_3 is the length of band between the platform and mirror, between the platform and inertial balancer, and between the inertial balancer and mirror. In addition, the potential energy by gravity is following that

$$\begin{aligned} V_{gM} &= -(\underline{m_o} + \underline{m}) \cdot m_M \, g(-\underline{k}), \\ V_{gG} &= -\underline{g_o} \cdot m_G \, g(-\underline{k}), \\ V_{gB} &= -\underline{b_o} \cdot m_B \, g(-\underline{k}), \\ V_{gP} &= -(\underline{P_o} + \underline{P}) \cdot m_P \, g(-\underline{k}). \end{aligned} \tag{3.4}$$

Thus, the potential energy V of the gimbal system is the sum of (3.3) and (3.4).

$$V = V_k + V_{gM} + V_{gG} + V_{gB} + V_{gP} \tag{3.5}$$

The generalized forces include the forces varying according to the working time and the non-conservative forces unable to derive from potential energy. The generalized coordinates q_i are the rotation angle θ_G, θ_P and θ_B, and the generalized forces with respect to the generalized coordinates are represented as follows.

$$\begin{aligned} Q_{\theta_G} &= T_{mG} - \tau_{fG}, \\ Q_{\theta_P} &= T_{mp} - \tau_{fP}, \\ Q_{\theta_B} &= -\tau_{fB}, \\ Q_{\theta_M} &= -\tau_{,fM} \end{aligned} \tag{3.6}$$

where T_{mG} and T_{mP} indicates the external torques of rotating the gimbal housing at azimuth and of rotating the platform at elevation. The angular contact ball bearing is installed on the rotation shaft of the gimbal housing and the friction of bearing can be changed by pre-pressure and lubricant which are excited in the assembly of the system.

3.2 Simplification

The equations of motion are solved to use the Lagrange equation (3.1) and the nonlinear equations of motion for generalized coordinates θ_M, θ_P, θ_B and θ_G are given as follows [3].

The above nonlinear equation can be simplified by the following assumptions.

First, there is no motion of base structure, that is,

$$V^s = \omega^s = 0.$$

Second, the stiffness of wire band is infinite, for the identification of friction is achieved within the low frequency range, that is,

$$r_B \theta_B = r_M \theta_M = r_p \theta_p.$$

Also the gimbal system is decoupled at each direction, i.e., it can be driven independently. Therefore, the simplified equations of motion are obtained as

follows

$$J_A\ddot{\theta}_G+\tau_{fG}=T_{mG}, \tag{3.7}$$

$$J_E\ddot{\theta}_P+\tau_{fE}=T_{mP}, \tag{3.8}$$

where J_A and J_E are the inertial moment, and τ_{fG} and τ_{fE} are the friction at each direction. The azimuth and elevation inertial moment are represented as follows

$$\begin{aligned}J_A=\ & G_3+B_3+P_3+M_3/2+M_2/2+m_Bb_2^2+m_Cg_2^2\\ & +m_Mm_2(m_2+m/\sqrt{2})+m_pb_2(b_2-p)\end{aligned} \tag{3.9}$$

$$J_L=P_1+m_pb^2+(M_1+m_Mm^2)\left(\frac{r_M}{r_p}\right)^2+B_1\left(\frac{r_B}{r_p}\right)^2 \tag{3.10}$$

4. LMI-based H_∞ Controller Design

4.1 Preliminaries

This is concerned with the standard H_∞ control problem. Given a linear time-invariant plant $P(s)$ with state-space equations [10], and the references therein.

$$\begin{aligned}\dot{x} &= Ax + B_1w + B_2u,\\ z &= C_1x + D_{11}w + D_{12}u,\\ y &= C_2x + D_{21}w,\end{aligned} \tag{4.1}$$

the γ-suboptimal H_∞ synthesis problem consists of finding an internally stabilizing controller $u = K(s)y$ that makes the closed-loop L_2 gain from the disturbance w to the error signal z less than γ. If $T_{wz}(s)$ denotes the closed-loop transfer function from w to z, this control objective can be formalized as

$$\| T_{wz} \|_\infty < \gamma, \tag{4.2}$$

where the H_∞ norm of a stable transformation is defined as its largest gain across frequency :

$$\| G(s) \|_\infty := \sup \sigma_{\max}(G(j\omega))$$

In this standard formulation, one of the H_∞ problem is a disturbance attenuation. Throughout this paper, we only assume that (A, B_2, C_2) is stabilizable and detectable. Singular plants with $j\omega$-axis zeros in $P_{12}(s)$ or $P_{21}(s)$ or rank deficiencies in D_{12} or D_{21} are therefore encompassed by this approach. The problem dimensions are summarized by $A\in \boldsymbol{R}^{n\times n}$, $D_{11}\in \boldsymbol{R}^{p_1\times m_1}$, $y\in \boldsymbol{R}^{p_2}$, $u\in \boldsymbol{R}^{m_2}$.

For brevity, we only discuss the computation of ful l-order H_∞ controllers, i.e., the controllers of the same order n as the plant.

Given a realization

$$K(s)=D_K+C_K(sI-A_K)^{-1}B_K, A_K\in \boldsymbol{R}^{n\times n} \tag{4.3}$$

of the controller $K(s)$. a realization of the closed-loop transfer function from w to z is given by

$$T_{wz}(s)=D_{cl}+C_{cl}(sI-A_{cl})^{-1}B_{cl}$$

where

$$\begin{aligned}A_{cl}&=\begin{pmatrix}A+B_2D_KC_2 & B_2C_K\\ B_KC_2 & A_K\end{pmatrix}\\ B_{cl}&=\begin{pmatrix}B_1+B_2D_KD_{21}\\ B_KD_{21}\end{pmatrix},\\ C_{cl}&=(\,C_{1+D_{12}}D_KC_2 \quad D_{12}C_K),\\ D_{cl}&=(\,D_{11}+D_{12}D_KD_{21}).\end{aligned} \tag{4.4}$$

We now briefly review the LMI-based H_∞ approach to H_∞ synthesis. The bounded real lemma, interval stability and the H_∞ norm constraint are jointly equivalent to the existence of $X_{cl} > 0$ of dimensions $2n\times 2n$ such that

$$\begin{pmatrix}A_{cl}^TX_{cl}+X_{cl}A_{cl} & X_{cl}B_{cl} & C_{cl}^T\\ B_{cl}^TX_{cl} & -\gamma I & D_{cl}^T\\ C_{cl} & D_{cl} & -\gamma I\end{pmatrix} < 0 \tag{4.5}$$

where the unknown matrices are the Lyapunov matrix X_{cl} and the controller matrices entering in A_{cl}, B_{cl}, C_{cl} and D_{cl}.

Hence, solving(4.5) is not an LMI problem.

However, this can be reduced to an LMI problem by the elimination of the controller matrices. With the notation

$$\Omega_K := \begin{pmatrix} A_K & B_K \\ C_K & D_K \end{pmatrix} \tag{4.6}$$

the inequality (4.5) can be written as

$$Z + P^T \Omega_K Q + Q^T \Omega_K^T P < 0 \tag{4.7}$$

where the matrices Z, P and Q depend only on X_{cl} and the plant data. We call this LMI in Ω_K the controller LMI.

Explicit formulas have been derived for LMI-based H_∞ controllers in continuous time contexts. These formulas are particularly suited for numerically stable implementation and bring insight into the controller structure [12]. They have been successfully implemented in the LMI Control Toolbox for use MATLAB [9].

4.2 Requirement for Controller Design

The H_∞ controller of the given system is designed to satisfy the necessary conditions for the design specification. In particular, the angular velocity must keep track with its operator's command.

The range of gimbal's motion must lie between -10°and 20°in the elevation direction on the installed side of the stabilized mirror, and must be -3°and 3°in the azimuth direction.

In case that the mirror is subjected to gun and turret, the static position accuracy from electrical signal to the LOS must be as follows.

Elevation : -10°< ε < 20° error △ ε :
Max. 0.25 mil

Azimuth : -3°< η < 3° error △ η :
Max. 0.20 mil

The stabilized head mirror must produce the minimum 10 °/s in the elevation and the minimum 40°/s in the azimuth.

In the limit of LOS tracking accuracy is angle between -10°and 20°at elevation, and between -3°and 3°at azimuth, The error of the excited velocity command and the real LOS velocity must not exceed the maximum 1.5 % or 0.3 mil/s.

The drift occurred by the stabilized gyro is adjusted on each axes in 5 minutes after the power is supplied, and then the mean of drifts which is measured after 5 minutes again must not exceed ±0.025 mil/s. The range of drift adjustment must not be smaller than ±1 mil/s. The bandwidth of this loop shouldn't be smaller than 30 Hz in both axes.

The bandwidth of this loop also should be at least 10Hz in both axes.

4.3 Formulation of LMI-based H_∞ Controller Problem

As previously satisfied with the design specification for H_∞ controller, the generalized plant is constructed as Figure 4.1.

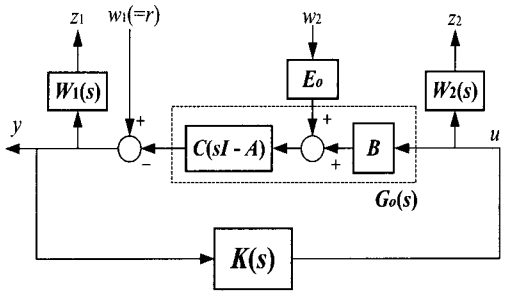

Fig. 4.1 The generalized plant for H_∞ controller design

where $G_o(s)$ is the nominal model including the motor and the gimbal as the control plant and $W_1(s)$ and $W_2(s)$ are the weighting functions for the input and output of $G_o(s)$ respectively and $K(s)$ is the designed H_∞ controller. Also, we define the reference input r and the plant input disturbances as the external input w_1 and w_2, the control objectives z_1 and z_2 as the error between the plant output and r and the control input u. In addition, the closed-loop transfer function $G_{zw}(s)$ from w_1, w_2 and u to z_1, z_2 and y is given as follows

$$\begin{bmatrix} z_1 \\ z_2 \\ y \end{bmatrix} = \begin{bmatrix} W_1(s) & W_1(s)E(s) & W_1(s)G(s) \\ 0 & 0 & W_2(s) \\ I & E(s) & G(s) \end{bmatrix} \begin{bmatrix} w_1 \\ w_2 \\ u \end{bmatrix} \quad (4.8)$$

where $E(s)$ is the transfer function from the disturbance w_2 to the plant output. By realizing the state variables for $G_o(s)$, $E(s)$, $W_1(s)$ and $W_2(s)$ into (4.9), the given generalized plant can be represented as the state space model [10], and the references therein.

$$G_o(s) = \begin{bmatrix} A_o & B_o \\ C_o & D_o \end{bmatrix}, E(s) = \begin{bmatrix} A_o & B_o \\ C_o & E_o \end{bmatrix},$$

$$W_1(s) = \begin{bmatrix} A_{w1} & B_{w1} \\ C_{w1} & D_{w1} \end{bmatrix}, W_2(s) = \begin{bmatrix} A_{w2} & B_{w2} \\ C_{w2} & D_{w2} \end{bmatrix} \quad (4.9)$$

$$\dot{x} = \begin{bmatrix} A_{w1} & 0 & -B_{w1}C_o \\ 0 & A_{w2} & 0 \\ 0 & 0 & A_o \end{bmatrix} x + \begin{bmatrix} B_{w1} & 0 \\ 0 & B_{w2} \\ 0 & E_o \end{bmatrix} w + \begin{bmatrix} 0 \\ 0 \\ B_o \end{bmatrix} u \quad (4.10)$$

$$z = \begin{bmatrix} C_{w1} & 0 & -D_{w1}C_o \\ 0 & C_{w2} & 0 \end{bmatrix} x + \begin{bmatrix} D_{w1} & 0 \\ 0 & 0 \end{bmatrix} w + \begin{bmatrix} 0 \\ D_{w2} \end{bmatrix} u \quad (4.11)$$

$$y = [\,0 \;\; 0 \;\; -C_o\,]\, x + [\,I \;\; 0\,]\, w \quad (4.12)$$

4.4 Simulation Results and Remarks

To compare the performance with the existing controller, we deal with two cases in the elevation direction; one is the case with disturbance and the other is under no disturbance. Figure 4.2 shows the step response characteristics of the proposed H_∞ controller, compared with that of the conventional PI-Lead controller under some disturbances. The maximum overshoot of H_∞ controller is 38 % and its settling time is 0.09 second, while the maximum overshoot of PI-Lead controller is 60 % and its settling time is 0.3 second. Thus, It can be known that this proposed H_∞ controller has better performance in step response under no disturbance. The step response is also considered under some disturbances. Figure 4.3 presents each step responses of PI-Lead controller and H_∞ controller when the angular velocity step disturbance 0.5 mil/sec is occurred at 1 second. In both controllers, the 0.5 mil/sec is decreased in the step response at that time, but PI-Lead controller has a steady state error at 0.21 second and H_∞ controller has it in 0.06 second respectively after the disturbance entered. Therefore, it can be known that the disturbance rejection of H_∞ controller is so good in the control performance.

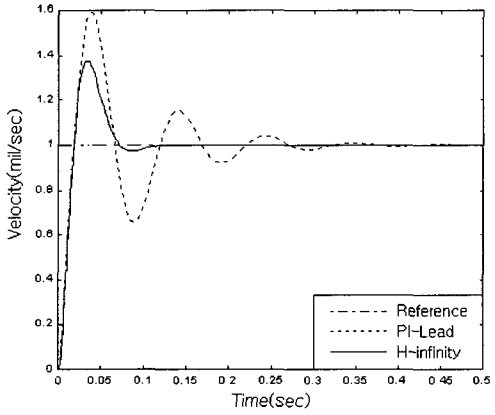

Fig. 4.2 Step response without disturbances

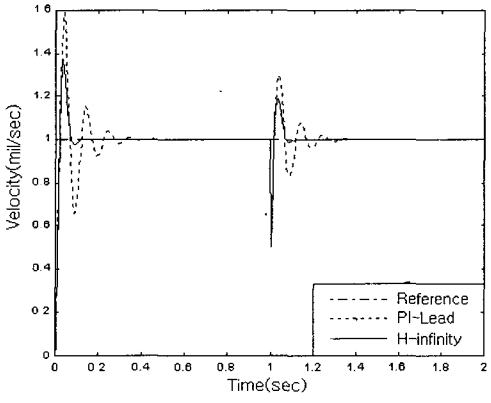

Fig. 4.3 Step response under step type output disturbance

The simulations inspecting robust performances such as disturbance attenuation and reference input tracking are accomplished in the elevation direction. Figure 4.4 (a) shows that the maximum overshoot of the proposed is smaller than that of PI-Lead controller, but they have overall similar responses at 20 KPH in the paved road. However, the faster the velocity of the vehicle is, the worse the responses of PI-Lead controller while that of H_∞ is not so bad in Figure 4.4 (b). Also,

Figure 4.5 indicates that both responses of controllers have an inclination to be worse in faster motion, and badly shaped road because nonlinear factors of the system are more affected in faster motion than in slow motion.

In addition, as ill shaped road have worse effects on the vehicles' motion, their controllers can't have a good stabilization performance. Compared with the PI-Lead controller, H_∞ controller has better robust performance even against real disturbance and nonlinear uncertainty.

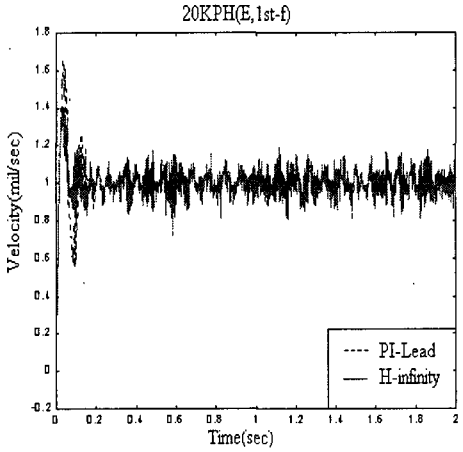

(a)

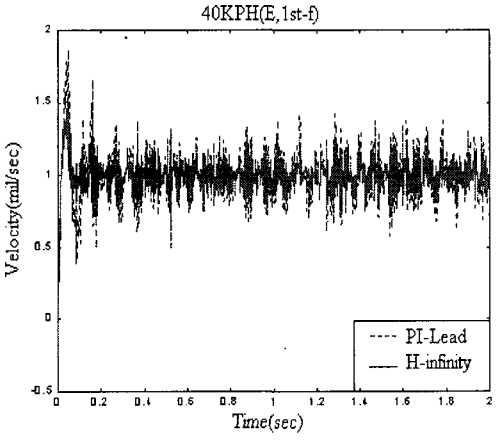

(b)

Fig. 4.4 Angular velocity response under paved road disturbances ((a) 16KPH (b) 32KPH)

Consequently, these results indicate that the proposed H_∞ controller has a better tracking performance for the reference input than that of the conventional PI-Lead controller under no disturbances. In addition, the proposed H_∞ controller has a better performance for disturbance attenuation and reference input tracking under any real disturbances.

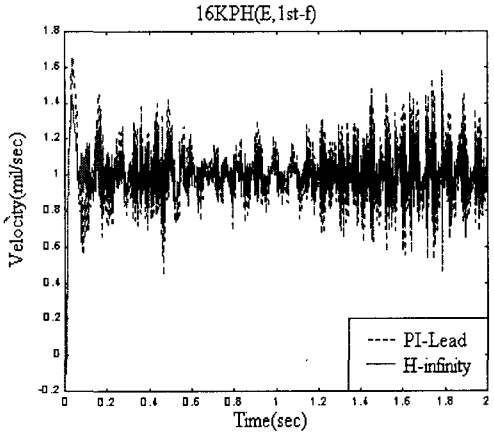

(a)

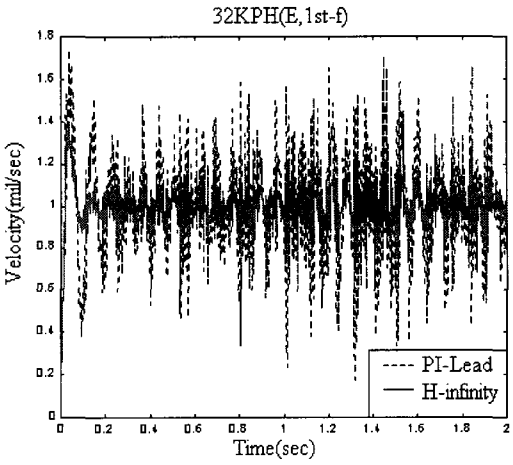

(b)

Fig. 4.5 Angular velocity response under bump course disturbances ((a) 16KPH (b) 32KPH)

5. Summary and Conclusions

5.1 Concluding Remarks

It is necessary to design the robust controller against the modeling error and disturbance, even where the applied LOS stabilization system can achieve the independent servo function and stabilization function and drive in two directions respectively. In this paper,

these nonlinear characteristics are investigated by the experiments such as the bandwidth, transient response and the mirror chattering in a halt, and the disturbances' effect on the system are scrutinized in time and frequency domain. In designing controller, we inspected the accurate dynamics of the system in order to keep a better LOS under a variety of disturbances, and proposed the results to assure the proposed control algorithm's performance after applying to the dynamic equations. In addition, we designed an LMI-based H_∞ controller to improve the control performance for robustness against the parametric changes, modeling errors and disturbances, and then accomplished the simulation with them. Based on the above control algorithm, the following results is obtained by the simulation.

First, it can be affirmed that the proposed \controller has the better control performances on nonlinear parametric change, modeling error and in particular, under any disturbances. Second, it has a stable tracking performance for input command of ballistic trajectory calculator for the angular velocity control of stabilization mode and the angle control of follow mode, and has more excellent stabilization performance in the azimuth direction for sinusoidal input than in the elevation. Third, we obtained a nice and well performance in time domain by the experiments after mounting the system on the track vehicle in driving on both paved and bump course. Finally, we concluded that the proposed LMI-based H_∞ controller had good disturbance attenuation and reference input tracking performance under the real disturbances, compared with the control performance of conventional controller under any real disturbances.

5.2 Suggestion for Further Research

To further improve the robust control for the track-vehicle's LOS stabilization system, there must be a progressive development of feasible algorithm and the improvement of the kinematic gimbal structure which can overcome the constraints for azimuth and elevation angle. Furthermore, the stability of the proposed robust controller must be scrutinized before applying this algorithm to real system under real disturbances.

References

1. M. Iecovich, "Line of Sight Stabilization Requirements for Target Tracking Systems," Proceedings of SPIE Acquisition, Tracking, and Pointing IV, Vol. 1304, pp. 100-111, 1990.
2. M. H. Lee, The Study on Stabilization Characteristic and Control of Stabilized Head Mirror, Final Report to Agency for Defense Development, 1990.
3. B. Li, D. Hullender, and M. Direnzo, "Active Compensation for Gimbal Bearing Friction in Vibration Isolation and Inertial Stabilization Problems," ASME Active Control of Vibration and Noise, DE-Vol. 75, pp. 471-476, 1994.
4. J. E. Keh, and M. H. Lee, "Sliding Mode Control of the Gunner's Primary Stabilized Head Mirror," Journal of the Korean Society of Precision Engineering, Vol. 10, pp. 109-117, 1999.
5. J. E. Keh, "Performance Evaluation and Robust Controller Design of a Line of Sight Stabilization System," Ph. D. Thesis, Pusan National Univ., 2000.
6. P. Gahinet, and P. Apkarian, "An LMI-based parametrization of all H∞ controllers with applications," Proceedings of IEEE Conference Decision and Control, pp. 656-661, December 1993.
7. S. Boyd, L. El Ghaoui, E. Feon, and V. Balakrisnan, Linear Matrix Inequalities in Systems and Control Theory, SIAM, Philadelphia, 1994.
8. P. Gahinet, and P. Apkarian, "A linear matrix inequality approach to H∞ control," International Journal of Robust and Nonlinear Control, Vol. 4, pp. 421-448, 1994.
9. P. Gahinet, A. Nemirouski, A. J. Laub, and M. Chilali, LMI Control Toolbox, Math Works, 1995.
10. J. C. Doyle, K. Glover, P. Khargonekar, and B. A. Francis, "State-space solutions to standard H2 and H∞ control problems." IEEE Transactions on Automatic Control, Vol. 34, No. 8, pp. 831-847, August 1989.
11. K. Zhou, and J. C. Doyle, Essentials of Robust Control, Prentice Hall, 1998.
12. Murat Zeren, and Hitay Ozbay, "On the Synthesis of Stable H∞ Controller," IEEE Transactions on Automatic Control, Vol. 44, No. 2, pp. 431-435, February 1999.